Article

Homology Model-Based Virtual Screening for the Identification of Human Helicase DDX3 Inhibitors

Roberta Fazi,[†] Cristina Tintori,[†] Annalaura Brai,[†] Lorenzo Botta,[†,‖] Manikandan Selvaraj,[†,⊥] Anna Garbelli,[‡] Giovanni Maga,[‡] and Maurizio Botta*[,†,§]

[†]Dipartimento Biotecnologie, Chimica e Farmacia, Università degli Studi di Siena, Via A. De Gasperi 2, I-53100 Siena, Italy
[‡]Istituto di Genetica Molecolare, IGM-CNR, Via Abbiategrasso 207, I-27100 Pavia, Italy
[§]Biotechnology College of Science and Technology, Temple University, Biolife Science Building, Suite 333, 1900 N 12th Street, Philadelphia, Pennsylvania 19122, United States

Ⓢ *Supporting Information*
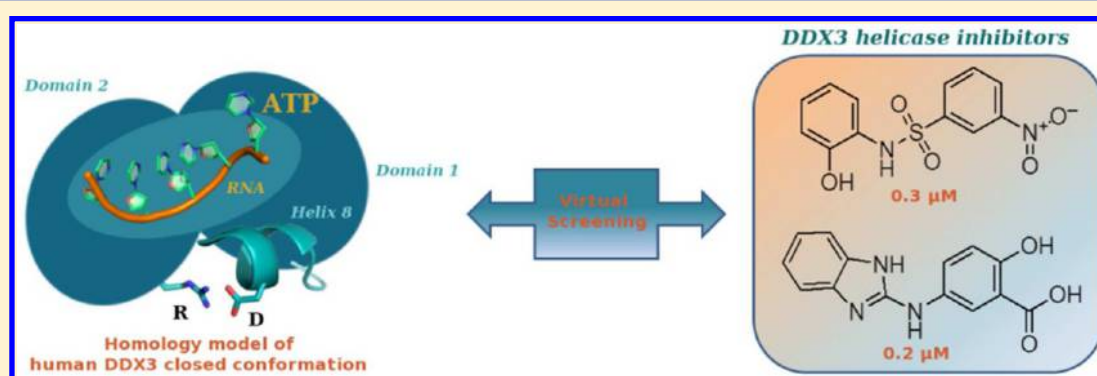
ABSTRACT: Targeting cellular cofactors instead of viral enzymes represents a new strategy to combat infectious diseases, which should help to overcome the problem of viral resistance. Recently, it has been revealed that the cellular ATPase/RNA helicase X-linked DEAD-box polypeptide 3 (DDX3) is an essential host factor for the replication of several viruses such as HIV, HCV, JEV, Dengue, and West Nile. Accordingly, a drug targeting DDX3 could theoretically inhibit all viruses that are dependent on this host factor. Herein, for the first time, a model of hDDX3 in its closed conformation, which binds the viral RNA was developed by using the homology module of Prime through the Maestro interface of Schrodinger. Next, a structure-based virtual screening protocol was applied to identify DDX3 small molecule inhibitors targeting the RNA binding pocket. As a result, an impressive hit rate of 40% was obtained with the identification of 10 active compounds out of the 25 tested small molecules. The best poses of the active ligands highlighted the crucial residues to be targeted for the inhibition of the helicase activity of DDX3. The obtained results confirm the reliability of the constructed DDX3/RNA model and the proposed computational strategy for investigating novel DDX3 inhibitors.

INTRODUCTION

Compounds currently used for the treatment of HIV infection target viral proteins. However, viruses have very high intrinsic mutation and replication rates that often lead to the emergence of drug resistant strains. As a consequence, significant effort is presently devoted to the development of novel antiviral agents with different mechanism of actions. Host cellular proteins are less prone to mutate than viral ones thus providing new targets of research in the field of antivirals, which could help to overcome the drug resistance issue.[1−3] The human DDX3 (or DBX), first identified in 1997, is an ATP-dependent RNA helicase belonging to the DEAD (Asp-Glu-Ala-Asp)-box family.[4] A role of DDX3 in HIV life cycle has been first proposed by Yedavalli and co-workers in 2004,[5] as a shuttling protein, which works within the Rev-RRE/CRM1 pathway and is responsible for the export of unspliced/partially spliced HIV RNAs from the nucleus to the cytoplasm. As a proof of such a mechanism, the knockdown of

DDX3 is associated with the inhibition of HIV replication as a consequence of the block of the HIV RNAs nucleo-cytoplasmic export.[6] Later studies also suggested a role of DDX3 in the translation of HIV-1 mRNAs.[7,8] Besides HIV, DDX3 is known to be an essential host factor for other major human viral pathogens such as Hepatitis B and C viruses.[9] Moreover, DDX3 also plays a key role in the replication of viral agents responsible for orphan diseases such as Dengue virus (DENV), West-Nile virus (WNV), and Japanese Encephalitis Virus (JEV).[10,11] On this basis, small molecule DDX3 inhibitors could be developed as drugs with multiple antiviral activities. The three-dimensional crystal structure of the human RNA-free conformation of DDX3 has been solved in 2006 in complex with AMP (PDB code: 2I4I).[12] It consists of two domains (named 1 and 2) connected by a short
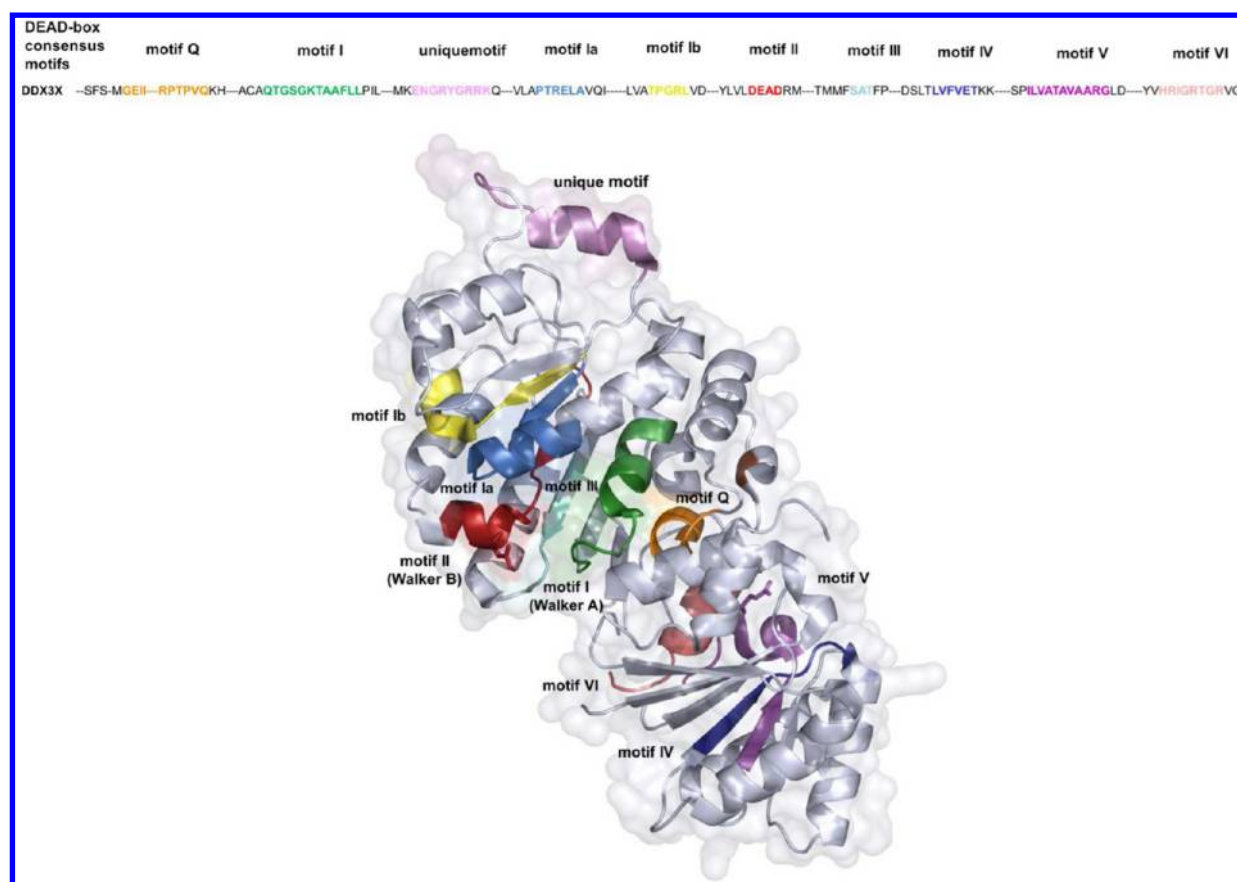
Figure 1. Nine conserved motifs of the DEAD-box family are highlighted with different colors in the FASTA sequence (upper) and in the 3D cartoon representation of hDDX3X open conformation in complex with AMP (down): motif Q (orange), motif I (forest green), unique motif (violet), motif Ia (marine), motif Ib (yellow), motif II or DEAD motif (firebrick), motif III (aquamarine), motif IV (deep blue), motif V (purple), and motif VI (salmon).
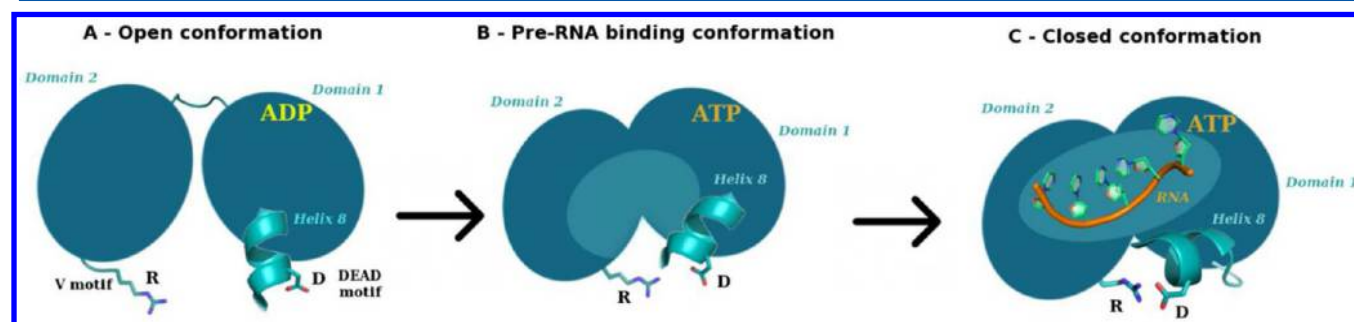

Figure 2. Schematic model proposed by Schüler et al. for the RNA binding site activation. The structural mechanism for unblocking the RNA binding site involved a transition between different conformational states at each catalytic cycle depending on ATP and RNA binding. (A) Open conformation: in the free substrate state, subdomains are separated and the RNA binding site is partway covered by α-helix8 (ended segment of DEAD-motif). The pictured aspartate is the terminal residue of the DEAD sequence, while the arginine highlighted in domain 2 is a conserved residue of motif V. (B) Pre RNA-binding conformation: the ATP binding promotes the closure of the cleft partially unblocking the RNA binding site by rotation of α-helix 8. (C) Closed conformation: RNA binding complete the cleft closure. A salt bridge stabilizes the closed conformation.

flexible linker and shows all the nine conserved motifs that characterize the DEAD-box superfamily 2 members (Figure 1). Both domains contribute to ATP hydrolysis and RNA binding. The N-terminal domain 1, or DEAD domain, contains the ATP binding Motifs Q, I (Walker A) and II (Walker B), and the RNA-binding Motifs Ia, Ib and III. Domain 1 also includes a nuclear export signal (NES) and a specific insertion of ten amino acids between motifs I and Ia, namely unique motif, which is not found in other DEAD-box helicases. The carboxyl-terminal domain 2 or helicase domain contains the RNA-binding Motifs IV and V as well as the Motif VI, which it was shown to be

important for both ATPase activity and RNA binding. In solution DDX3 could exist in either an open or a closed conformation, with a transition between the two states at each catalytic cycle depending on ATP and RNA binding. The structural mechanism for the linkage between binding of ATP and activation of the RNA binding site has been recently proposed by Schütz et al.[13] (Figure 2) and is characterized by three distinct conformational states named open, pre-RNA binding and closed conformation. The DDX3 open conformation (Figure 2A), which corresponds to that solved in the 2I4I crystal structure,[12] is not able to bind the RNA substrate because the α-helix 8 of the DEAD-motif partially

blocks the helicase pocket. After ATP binding the helicase domain 2 rotates by about 180° with respect to domain 1 generating a compact pre-RNA binding conformation (Figure 2B). Next, RNA binding to the DEAD-domain completes cleft closure allowing the placement of α-helix 8 out of the RNA binding site (Figure 2C). The closed or RNA binding competent conformation is stabilized by a salt-bridge between the conserved arginine of motif V (Arg 503) and the aspartic acid of the DEAD-motif (Asp 350), which is the terminal residue of α-helix 8. Furthermore, still according to the comparative structural analysis performed by Schütz et al.,[13] ATP hydrolysis and phosphate release switches the α-helix 8 back to the original conformation, allowing the release of the RNA substrate. From a medicinal chemistry point of view, DDX3 has multiple enzymatic activities (ATPase and RNA helicase) and functional domains that may be targeted by potential inhibitors. The first small molecules designed to inhibit the ATPase activity of DDX3 has been identified by our research group.[14−17] However, the major limit of such ATP-mimetics could be represented by poor in vivo selectivity. Accordingly, in continuing efforts to identify novel DDX3 inhibitors, we discovered the first small molecule inhibitors of HIV-1 replication (in peripheral blood mononuclear cells infected with HIV-1) specifically designed to target the DDX3 RNA binding site.[18,19] Pursuing this research line, herein we report the development of a 3D structure of DDX3 in its RNA-bound closed conformation obtained by homology modeling together with its validation in a virtual screening protocol, which led to the identification of submicromolar hDDX3 helicase inhibitors.

■ METHODS

Homology Modeling. The protein sequence of human DDX3 was obtained from the protein NCBI database. Sequence similarity search with BLAST in Protein Data Bank has highlighted the Drosophila Vasa DEAD-box helicase (PDB code: 2DB3, 2.20 Å resolution)[20] as the most similar protein after that of human DDX3 that was however crystallized in its open conformation (PDB code: 2I4I).[12] The 3D structure of Drosophila Vasa was crystallized in its closed RNA-bound conformation and it showed a FASTA sequence identity of 44% with the human DDX3. The homology model was built by means of the software PRIME accessible through the Maestro interface (Schrodinger, Inc.).[21] The crystal structure of Drosophila Vasa DEAD-box helicase was used as the first template while the open conformation of human DDX3 (PDB ID: 2I4I) was selected as the second template to fill the residues belonging to the unique motif of DDX3, which are missing in the 2DB3 structure. The sequence alignment used is shown in the Supporting Information (Figure S1). All other PRIME parameters were set to their default values. Next, explicit hydrogens were added to the protein and the system subjected to energy minimization using the Macromodel force-field OPLS-2005[22] and the Polak-Ribiere conjugate gradient algorithm. The minimization was terminated when the rms energy gradient reached a value of 0.01 kJ Å^{-1} mol^{-1}. Model evaluation was performed producing the Ramachandran plot (Figure S2 in the Supporting Information). Furthermore, molecular dynamics simulations were performed on the model of hDDX3 in the presence of ATP or AMP, which confirm the reliability of the generated structure (see the Supporting Information).

Pharmacophore Screening. Two structure-based pharmacophore models were built with LigandScout v3.1 starting from the complex between hDDX3 and the active ligand **1** previously

obtained by docking studies (see the Docking Studies section below for details) and using default settings. The pharmacophore models generated by LigandScout v3.1[23] were then used for the screening of commercial databases including: Asinex (www.asinex.com), Chembridge (www.chembridge.com), Inter-BioScreen (www.ibscreen.com), and SPECS (www.specs.net). These databases were downloaded in SDF format from the Web and converted into a database of 3D structures with the idbgen command. A conformational model consisting of a maximum of 250 conformers was generated for each compound so as to reproduce the flexibility of molecules during the database search. The resulting databases were stored in the LigandScout database format (LDB). The database search by means of the pharmacophore models was performed with LigandScout v3.1 by using the Iscreen module.

Docking Studies. All compounds studied herein were docked within the RNA binding site of the modeled hDDX3 closed conformation using the software package GOLD 4.1.[24,25] The pocket under investigation was inserted into a grid box centered on residue Phe357 and enclosing residues lying within 10 Å from such amino acid. The genetic algorithm parameter settings were employed using the search efficiency set at 100%, and 100 runs were carried out for each ligand. Chemscore was chosen as the fitness function. Finally, results differing less than 1.5 Å in ligand-all atom RMSD were clustered together. For each putative inhibitor, the first ranked solution was selected for further analysis. Visual analysis of the docked pose of compounds and their agreement to pharmacophore mapping were considered in selection of the compounds. Complexes between hDDX3 and active ligands **1**, **14**, **24**, and **25** were in turn refined by means of the Refine Protein−Ligand complex utility included in Maestro Schrodinger Suite. Pictures of the modeled ligand−enzyme complexes together with graphic manipulations were rendered using the PyMOL molecular graphic system.[26]

Compounds Analysis. Purity of compounds was reported by vendors ranging from 93% to 99%. To check for this degree of purity, we perform a HPLC analysis of compounds after shipping and storage. Solutions were analyzed, finding percent purity values comparable to those reported by vendors. ^{1}H NMR spectra were recorded to confirm that compounds have the reported structure.

Biological Test. The inhibition of DDX3 helicase activity by the selected compounds was monitored as previously reported by measuring the conversion of a double stranded (ds) RNA (labeled at the 5′-end of one strand with a 6-FAM fluorescent) into single stranded (ss) nucleic acid. A final concentration of 10 nM RNA substrate was used in the experiments. Reactions were performed in 50 mM TrisHCl pH 7.5, 1 mMDTT, 0.2 mg/mL BSA, 5% glycerol, 3 mM MgCl$_2$ and 1 mM ATP, at 37 °C degrees for 30 min and stopped by adding EDTA 50 mM pH 8. Products were separated on a native 7% PAGE containing 0.1% (w/v) SDS at 5 W in TBE buffer with 0.1% SDS at 4 °C for 2 h. Substrates and products were quantified by laser scanning densitometry (Thyphoon-TRIO, GE Healthcare).

Kinetic Analysis. The IC$_{50}$ values have been calculated from dose−response curves. Data (in triplicate) were plotted and analyzed by least-squares nonlinear regression, according to the method of Marquardt−Levenberg, with the computer program GraphPad Prism 5.0. Data were fitted to the following equation:

$$E_{(obs)} = E_{(max)}/(1 + (IC_{50}/[I])^n) \qquad (1)$$

where $E_{(obs)}$ is the observed enzymatic activity in the presence of each inhibitor dose [I]; $E_{(max)}$ is the maximal enzymatic activity in
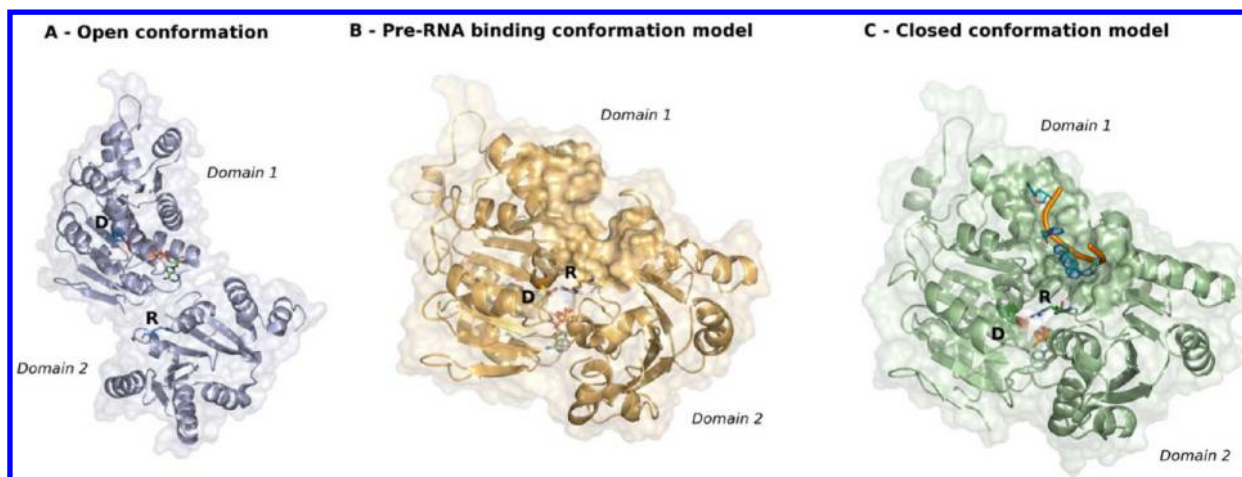
Figure 3. Cartoon and transparent surface representation of three different conformations adopted by DDX3 during the RNA binding site activation. (A) Open conformation: solved crystal structure of hDDX3 (PDB code 2I4I). Domain 1 and domain 2 are shown, and the AMP is represented as green carbons stick. Aspartate (D) belongs to the DEAD motif and Arginine (R) of motif V are highlighted. No interactions between the two residues are observed. (B) Pre RNA-binding conformation: pre-RNA binding model previously proposed by our group.[19] The RNA pocket is not completely open (C) Closed conformation: homology model of the closed hDDX3 conformation obtained herein. The RNA strain is placed in the competent binding site. Aspartate and arginine form a salt bridge that stabilize the closed conformation.

the absence of the inhibitor; n is an exponential term to take into account sigmoidal dose−response curves.

For the analysis of the mechanism of action and K_i calculation, IC_{50} values have been determined at different fixed doses of RNA substrate. The corresponding ID_{50} values calculated by eq 1 were then plotted as a function of the RNA substrate concentrations. Data were fitted to the modified form of the Cheng−Prusoff equation:

$$IC_{50(obs)} = K_i(1 + ([S]/K_m)^n) \qquad (2)$$

Where $IC_{50(obs)}$ is the inhibitory potency observed at each substrate concentration $[S]$; K_i is the apparent equilibrium dissociation constant for the enzyme−inhibitor complex, K_m is the apparent Michaelis constant for enzyme−substrate complex dissociation; n is an exponential term to take into account non linear dose−response curves.

RESULTS AND DISCUSSION

Homology Modeling. As mentioned above, DDX3 needs to switch through three different conformational states to carry out its functions (Figure 3): at the beginning, the open conformation is totally unsuitable to bind the RNA substrate; in the second step, after ATP-binding, the α-helix 8 starts to move out from the RNA-pocket, aimed to obtain a more stable conformation namely pre-RNA binding state. Finally, in the last step, which occurs after RNA binding, the conserved arginine (R503) of motif V forms a salt bridge with the aspartic acid of the DEAD-motif (D350), which is also the terminal residue of α-helix 8. This interaction stabilizes the closed conformation, where the α-helix 8 is rotated out of the RNA binding site to allow the placement of the substrate. At present a crystal structure of hDDX3 in complex with AMP is available in Protein Data Bank (PDB code: 2I4I)[12] representing the open conformation. Conversely, no experimental structures of hDDX3 in pre-RNA binding or RNA-bound closed states are available. Recently, a theoretical 3D structure of hDDX3 in its pre-RNA binding conformation has been generated by us[18] by aligning each individual domain of the 2I4I structure (domains 1 and 2) on the closed conformation of the DEAD-box helicase eIF4AIII for which a crystal structure was

available (PDB code: 2J0S).[27] The pre-RNA hDDX3 model was then used to perform a virtual screening approach, which led to the identification of the first hDDX3 helicase inhibitors able to inhibit the helicase activity of hDDX3 at low micromolar concentration. Among them, compound **1** and **2** proved to inhibit the helicase activity of DDX3 with IC_{50} values of 1 and 5 μM, respectively (Chart 1).

Chart 1. Structure of the Hit Compounds 1−2 Previously Identified As Human DDX3 Helicase Inhibitors[19]
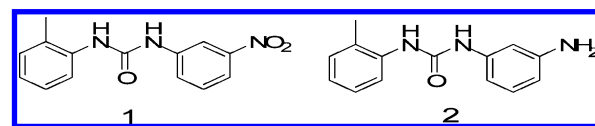
Despite the replacement of the amino group of **2** with the nitro group of **1** leading to a 5-fold improvement in inhibitory potency against the helicase activity of DDX3, the predicted binding pose within the pre-RNA binding pocket did not detect any polar interactions involving the nitro group. Conversely, a hydrogen bond interaction was found between the Gln360 side chain and the amino group of compound **2**. Starting from this observation, herein, we further explore the molecular interactions at the basis of **1** helicase inhibitory activity with the secondary aim of identifying new DDX3 inhibitors. To this aim, we first constructed the hDDX3-RNA complex (cited above as hDDX3 closed conformation) by means of a homology modeling approach. The crystal structure of *Drosophila* DEAD-box helicase Vasa (PDB code: 2DB3)[20] in complex with AMPPNP (a nonhydrolyzable analog of ATP) and a single stranded RNA was selected as main template because of its high degree of sequence homology and identity with hDDX3 (68% and 48%, respectively). A gap between the two FASTA sequences was detected, which corresponds to the DDX3 unique motif (aa 250−259). The hDDX3 open conformation (PDB code: 2I4I)[12] was used as the second template in order to fill this specific hDDX3 insertion of residues, which forms a helix. Remarkably, a comparison between the structure of the DEAD-box protein VASA bound to poly(U) RNA and the in silico modeled
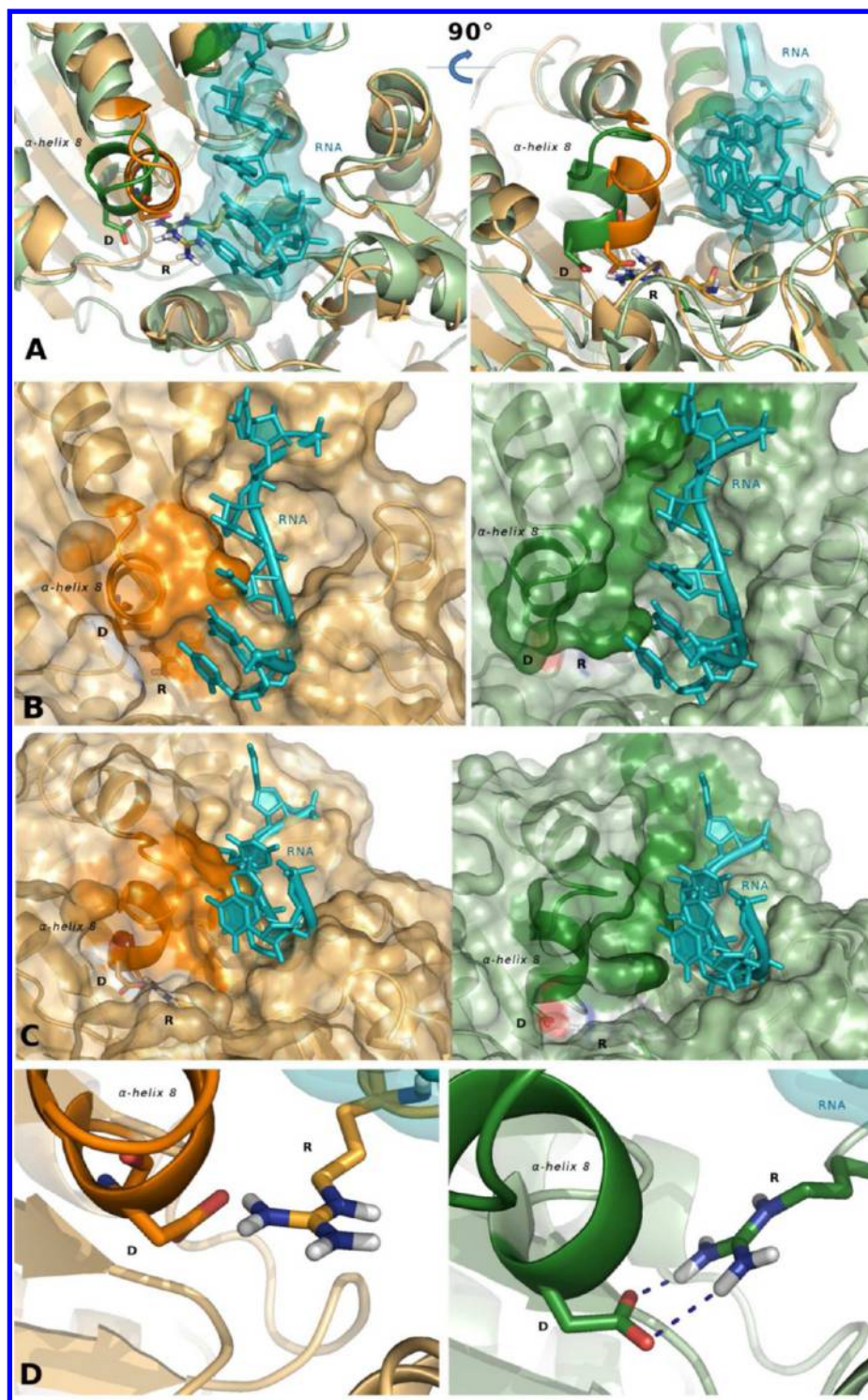
Figure 4. Details of RNA pocket in pre RNA-binding and closed DDX3 models. (A) Front view and 90° rotated view of superimposed pre RNA-binding (orange) and closed (green) DDX3 models. RNA is shown in dark cyan, stick, and transparent surface representation. Aspartate (D) and Arginine (R) involved in the salt bridge and α-helix 8 are highlighted. (B and C) Surface representation of RNA binding site of the two homology models. Note that in pre RNA-binding model (left side, orange) α-helix 8 would clash with the RNA substrate, while in the closed model (right side, green) no bad contacts were detected. (D) Details of the salt bridge between Aspartic acid and Arginine. Note that in pre RNA-binding model residues are not closed enough and correctly oriented to form a stable interaction.

RNA-bound closed conformation of DDX3 (amino acids 136−572) revealed that all amino acids involved in RNA binding are conserved among the two structures suggesting a common mechanism for RNA binding and the reliability of our model for the design of DDX3 inhibitors targeting the RNA pocket.

The crucial structural elements required for the DDX3 helicase activity could be highlighted by a comparative structure analysis between the generated closed conformation and the 3D structure of the pre-RNA binding state previously built.[18] Few significant differences were discovered in the shape of RNA-binding pocket,

in the position of α-helix 8 and in the salt bridge formation state (Figure 4). In detail, the RNA pocket of pre-RNA binding model is still closed and thus unable to accommodate the RNA strain. Conversely, in the new model presented herein the RNA substrate perfectly filled into a well formed pocket. Accordingly, in pre-RNA binding model (Figure 4, orange) the RNA binding site is still partially covered by the α-helix 8 of the DEAD-motif, while in the closed model (Figure 4, green), α-helix 8 has moved out of the RNA pocket. In addition, the two residues involved in the salt bridge that stabilize the RNA-binding competent conformation, show a quite different orientation in the two models. Because of the arrangement of the α-helix 8, in the pre-RNA model Arg503 and Asp350 are close to each other but unable to form a stable salt bridge. Vice versa, in the model of the closed conformation, the two residues are in the correct placement to make stable interactions and form a permanent salt bridge (see molecular dynamics paragraph in the Supporting Information).

Docking Studies on Hit Compound 1. Docking studies were conducted on hit compound **1** within the RNA binding pocket of the closed hDDX3 conformation after removal of the
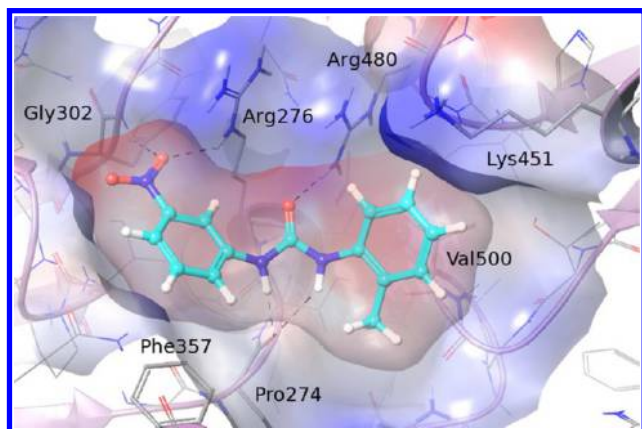

Figure 5. Graphical representation of the predicted binding mode of compound **1** (cyan), in the RNA binding site of the closed hDDX3 conformation. For the sake of clarity, only a few key residues are labeled and hydrogen bonding interactions are represented by black dashed lines. Compounds and key amino acids are shown in stick representation. Ligand and protein electrostatic surfaces are also visualized.

nucleic acid. The lowest energy conformation obtained was associated with a docking score of 31.40, higher than those previously obtained for the same compound into the pre-RNA binding conformation that was of 28.58. While docking is not always accurate in ranking different chemical structures it could be rather reliable to compare conformations of the same ligand—protein complex. Accordingly, it is reasonable to deduce that **1** preferentially targets the closed hDDX3 conformation. The predicted binding mode of **1** in the closed hDDX3 is shown in Figure 5. The **1**-hDDX3 optimized complex (see the Methods section for details) was stabilized by both polar and hydrophobic interactions. The two urea NH-groups of the inhibitor establish hydrogen bonds with the backbone carbonyl oxygen of Pro274 while the ureidic carbonyl group is involved in polar contacts with the side chain of Arg480. The nitrophenyl ring fills a hydrophobic cavity formed by Arg276, Gly302, and Phe357 where makes hydrogen bondings with Arg276 and Gly302. Furthermore, the tolyl moiety was accommodated within a mostly hydrophobic cavity delimited by the side chains of Arg480, His472, Gly473, Lys451, Thr498, Val500, and Ala499. A good electrostatic potential complementarity between protein and ligand was also observed especially involving Arg276 and Arg480 with nitro group and ureidic carbonyl moiety, respectively. Remarkably, most of the ligand contacts are coincident with the key interactions made by the RNA strain within the pocket. The DDX3 protein forms many hydrophilic interactions with both phosphate and 2'-OH groups of the RNA backbone. In detail, RNA phosphate backbone takes important contacts into the cavity with Arg276, Gly302, Thr323, Arg326, Lys451, Gly473, Arg480, and Thr498 while the ribose hydroxyl groups interact with Pro274, Gly325, Arg326, and Glu449. Finally, Arg351 and Gln360 were involved in hydrogen bond contacts with the base moieties of RNA substrate.

Virtual Screening. Starting from the docking pose of compound **1** within the RNA binding site of the hDDX3 in its closed state, a structure-based pharmacophore model was generated by means of the LigandScout software and was used as a query to perform a virtual screening of commercial databases, followed by docking experiments. Accordingly, the key interactions for the binding of **1** to hDDX3 were converted into a pharmacophoric hypothesis. The resulting model shown in Figure 6A is characterized by seven features: two hydrogen bond
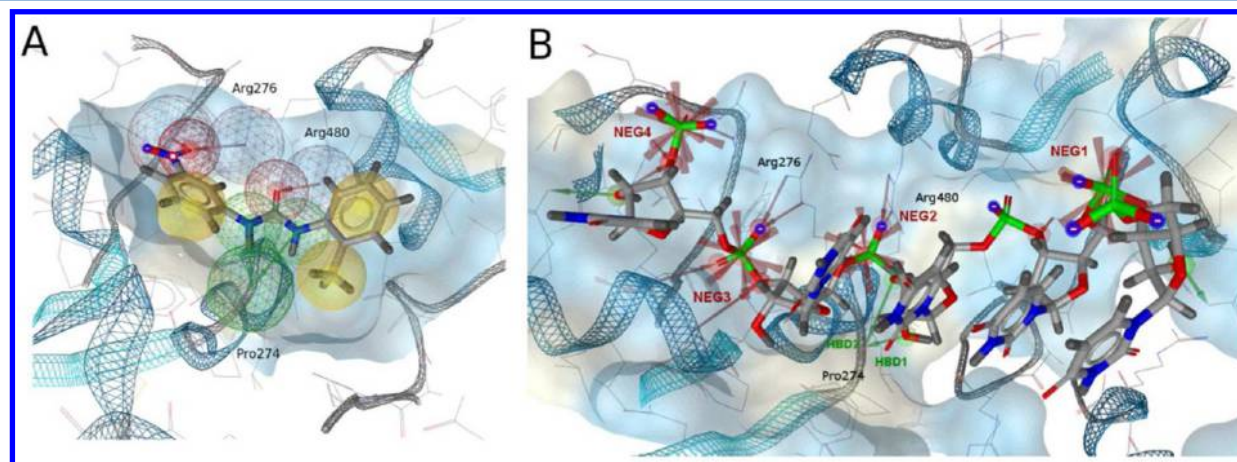

Figure 6. Structure-based pharmacophore models generated using LigandScout from homology model of DDX3 close conformation in complex with compound **1** (left) and the RNA stain (right), respectively. Hydrophobic groups (light yellow spheres), H-bond donors (green arrow), and H-bond acceptors (red arrow) are shown.

Table 1. Chemical Structures and Enzymatic Activity of Compounds 3−27 Selected from Commercial Databases by Docking Studies within the RNA Binding Site of hDDX3 along with Calculated QikProp Properties and Ligand Efficiency
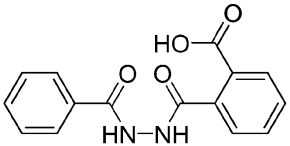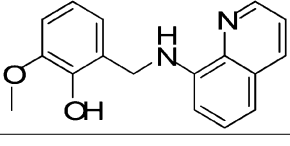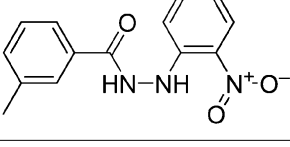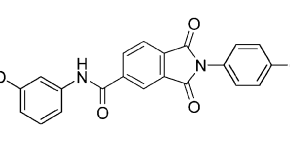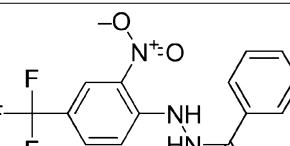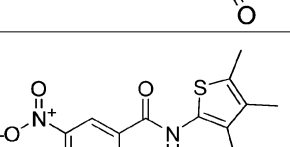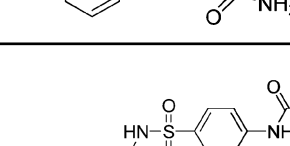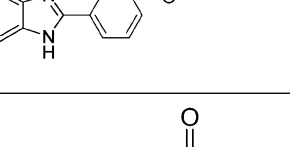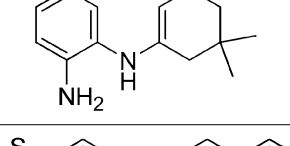
Name	Chemical Structure	IC$_{50}$ (µM)^a	Commercial code	QPlogS^b	QPlogP$_{o/w}$^{c}	QPP$_{caco}$ [nms^{-1}]^d	LE [Kcal(mol·N HA)$^{-1}$]
3		>200	Asinex BAS00569365	-3.119	2.434	93.352	< 0.24
4		97	Asinex BAS05346780	-3.807	3.328	2351.729	0.26
5		>200	Asinex BAS00605530	-3.929	2.148	282.585	< 0.25
6		156	Asinex BAS00298315	-5.391	2.823	153.698	0.18
7		7	Asinex BAS00313098	-4.736	2.989	318.065	**0.31**
8		17.5	Asinex BAS00541498	-4.235	1.791	63.642	0.29
9		>200	Asinex BAS00844166	-6.39	2.802	158.044	<0.17
10		6.6	Asinex BAS03161011	-2.949	1.993	744.584	**0.42**
11		>200	Asinex BAS04323716	-3.621	2.231	432.353	<0.25

Table 1. continued

Name	Chemical Structure	IC$_{50}$ (µM)[a]	Commercial code	QPlogS[b]	QPlogP$_{o/w}$[c]	QPP$_{caco}$ [nms^{-1}][d]	LE [Kcal(mol·NHA)$^{-1}$]
12		>200	Chembridge 5261271	-2.907	0.658	120.319	<0.24
13		>150	Chembridge 7779729	-3.435	1.136	93.899	<0.24
14		0.36	Chembridge 5227931	-2.875	0.846	77.472	**0.44**
15		9.6	Chembridge 5181912	-3.18	1.578	161.413	**0.36**
16		19.5	Chembridge 7989453	-4.293	2.706	343.97	**0.31**
17		15.4	IBS STOCK6S-20585	-1.037	0.342	49.387	**0.33**
18		>200	IBS STOCK6S-72571	-3.194	1.252	345.505	<0.25
19		>200	IBS STOCK3S-14656	-3.889	2.642	43.289	<0.23
20		61.3	SPECS AN-329/13193015	-3.129	1.646	904.339	**0.30**

Table 1. continued

Name	Chemical Structure	IC$_{50}$ (µM)^a	Commercial code	QPlogS^b	QPlogP$_{o/w}$^{c}	QPP$_{caco}$ [nms^{-1}]^d	LE [Kcal(mol·NHA)$^{-1}$]
21	(chemical structure)	33.8	SPECS AG-690/36490010	-2.561	1.034	0.674	0.24
22	(chemical structure)	45	SPECS AQ-086/41476304	-2.961	1.924	91.12	**0.31**
23	(chemical structure)	31	SPECS AP-263/40222373	-4.638	2.774	294.786	0.18
24	(chemical structure)	0.2	SPECS AQ-086/43457605	-3.395	2.092	28.48	**0.46**
25	(chemical structure)	2	SPECS AG-205/08449028	-3.063	1.094	352.627	**0.41**
26	(chemical structure)	27.8	SPECS AK-968/41026362	-3.276	2.067	67.26	**0.3**
27	(chemical structure)	5.7	SPECS AN-329/40719029	-2.669	1.827	1099.264	**0.48**

^{a}Data represents the mean of two independent experiments. ^{b}Predicted aqueous solubility (QP logS): values less than −6 or greater than −1 are undesirable. ^{c}Predicted octanol/water partition coefficient (QP log P$_{o/w}$): range of recommended values = −2.0 − + 6.5. ^{d}Predicted apparent Caco-2 cell permeability (QPP$_{caco}$): a value < 25 is poor.

donors, which accounted for the interactions between the two ureidic NH groups and the Pro274, two hydrogen bond acceptors mimicking the contacts of ligand with Arg276 and Arg480, and three hydrophobic features occupied by the two aromatic rings and the ortho methyl group of **1**. Finally, 12 excluded volumes, localized in region of space where amino acid backbone or side chains lie, identify zones inaccessible to any potential ligand, thus reflecting possible steric restrictions. On the other hand, taking into consideration the electrostatic interactions between the positively charge residues of the binding pocket and the negatively charged RNA substrate, four negative ionizable features could be recognized (namely NEG1, NEG2, NEG3, and NEG4), which describe the interactions with residues Lys451, Arg480, Arg276, and Arg326 (Figure 6B). The alignment between compound **1** and RNA within the pocket shows a perfect overlap between the nitro group and the NEG1 area, suggesting that a negative ionizable feature could be placed in that pharmacophoric position as an alternative to the hydrogen bond acceptor involved in the interaction with Arg276. To further confirm the pharmacophoric features identified by

LigandScout as hot spots for interaction between hDDX3 and **1**, GRID Molecular Interaction Fields (MIFs)[28] were calculated into the RNA binding region of the protein. DRY (hydrophobic), N1 (neutral flat NH, e.g., amide), and O (sp^2 carbonyl oxygen) were selected as probes to explore hydrophobic interactions and to mimic hydrogen bond donor and acceptor groups, respectively. Points of minimum of MIFs (i.e., the points in which the interaction energy assumes the lowest values) were calculated for each probe, thus identifying the regions of most favorable interactions with the protein. As a result, the points of minimum of MIF corresponded to the pharmacophoric features identified by LigandScout.

Next, in order to identify chemical scaffolds with putative affinity toward the DDX3 RNA binding site, the pharmacophore was used as the three-dimensional query of a virtual screening approach. Many databases of commercially available compounds (Asinex, Chembridge, Maybridge, InterBioScreen, Specs) consisting of a total of 1 664 152 molecules were filtered with the aim of selecting molecules able to map at least four of the seven pharmacophoric features. The top 6563 compounds in terms of pharmacophore fit score were then submitted to docking studies by the Gold software. Based on score, cluster population size and visual analysis the compounds were prioritized. We excluded however molecules for which the binding mode obtained with ChemScore and the pharmacophore mapping pose were in disagreement. Finally, in silico pharmacokinetic properties of the compounds were predicted using the Qikprop module implemented in Maestro Schrodinger Suite. In particular, three descriptors were determined and analyzed: the predicted octanol/water partition coefficient (QP log P), the predicted aqueous solubility (QP log S), and the predicted Caco-2 cell permeability (QP Pcaco). Compounds finally selected were predicted to have QP log P, QP log S, and QP Pcaco values within the recommended range (Table 1). Twenty five compounds (**3−27**) were purchased and evaluated for their ability to inhibit the helicase function of hDDX3. Among them, six molecules were identified with IC$_{50}$ values ranging from 20 to 100 μM, and ten molecules showed IC$_{50}$s lower than 20 μM with the best inhibitors, **14**, **24**, and **25** being endowed with inhibitory activities of 0.36, 0.2, and 2 μM, respectively. The high hit rate of our approach in finding new hDDX3 helicase inhibitors validates the computational protocol confirming the goodness of molecular features identified as responsible for the inhibitory activity against hDDX3. At the same time, this result suggests a good drugability of the target.[29]

Figure 7 shows the binding mode of compounds **14** and **24** and **25** as representatives of the most promising scaffolds identified. The nitrobenzene oxygens of **14** (Figure 7A) made favorable hydrogen bond interactions with Arg276, Gly302, Arg326, and Gly325. Furthermore, hydrogen bonds were also found between the sulfonamide group and the two amino acids Pro274 and Arg480 as well as between the hydroxyl substituent and the residues Pro274 and Arg503. Finally, the predicted complex was stabilized by hydrophobic contacts with Phe357, Val500, and Arg503. The preferred binding pose of compound **24** (Figure 7B) showed that the salicylic moiety, matching the NEG1 area, was involved in extensive polar contact with the side chain of Arg276 and the backbone NHs of Gly302, Arg326, and Gly325. Moreover, the benzimidazole established a hydrogen bond with the carbonyl of Pro274. Finally, hydrophobic interactions involved residues Phe357, Val500, and Arg503. Despite compound **25** being less active compared to **14** and **24** of an order of magnitude, the analysis of its binding
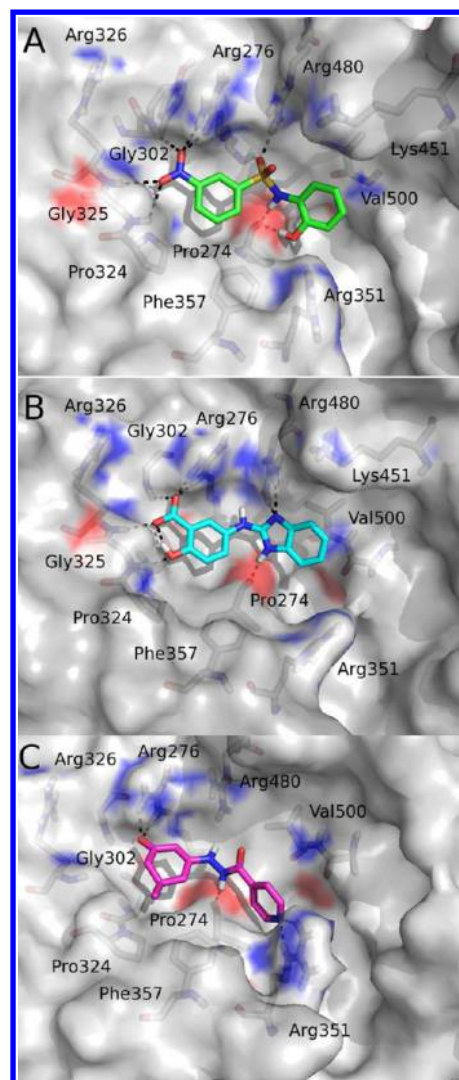

Figure 7. Graphical representation of the predicted binding mode of compounds (A) **14** (green), (B) **24** (cyan), and (C) **25** (magenta) into the RNA binding site of the closed hDDX3 conformation. For the sake of clarity, only a few key residues are labeled and hydrogen bonding interactions are represented by black dashed lines. Compounds and key amino acids are shown in stick representation.

mode (Figure 7C) is of interest because highlighted a different pattern of interactions. As well as compounds **14** and **24**, **25** showed hydrogen bond interactions with Arg276 and Pro274. However, unlike them, it was not involved in polar interactions with Arg480, Gly302, and Gly325 while it established a hydrogen bond with Arg351 through the pyridine ring. With regard to the hydrophobic interactions, **25** did not show profitable contacts with Val500 while efficiently interacted with Pro324. The structural information and binding site mapping of DDX3 for different inhibitors obtained from this study could aid in screening and designing of new broad spectrum antiviral agents targeting this enzyme. Furthermore, as a consequence of their small size, compounds **14**, **24**, and **25** are characterized by high ligand efficiency (>0.4), which made them good starting points for the development of more potent inhibitors in a process of hit-to-lead optimization. The ligand efficiency (LE) of **3−27** derivatives was calculated as the free energy of binding divided by the number of heavy atoms (non-hydrogen atoms, NHA) of the molecule. Values of 0.44, 0.46, and 0.41 kcal (mol NHA)$^{-1}$

were calculated for **14**, **24** and **25**, respectively, thus putting these compounds in a promising range for further optimization. It is important to highlight that compound **25** contains a hydrazide group, which is known to be unstable and prone to cleavage in the cell and thus particular attention will be focused on this aspect during its optimization toward new derivatives. Finally, compounds **14**, **24**, and **25** were docked within the RNA binding pocket of the pre-RNA DDX3 model. Similarly to compound **1**, higher score were measured for these hDDX3 helicase inhibitors into the closed form than within the pre-RNA conformation (33.128 vs 24.75, 28.320 vs 26.74, 26.62 vs 25.06, for compounds **14**, **24**, and **25**, respectively). The chemscore difference was rather pronounced for compound **14** which could be considered the best candidate for further optimization. Overall, the analysis of the interactions exploited by the active ligands identified herein within the RNA binding pocket will help the design of more potent helicase DDX3 inhibitors.

Validation of Mode of Action of Compound 14. The docking analysis described above suggested that compound **14** could block the RNA binding site of hDDX3. To experimentally validate this hypothesis, increasing amounts of compound **14** were titrated in helicase assays in the presence of hDDX3 and increasing fixed doses of RNA substrate. The corresponding dose−response curves, along with the computed IC_{50} values, are shown in Figure S7 of the Supporting Information. As can be seen from Figure 8, the apparent potency of inhibition decreased
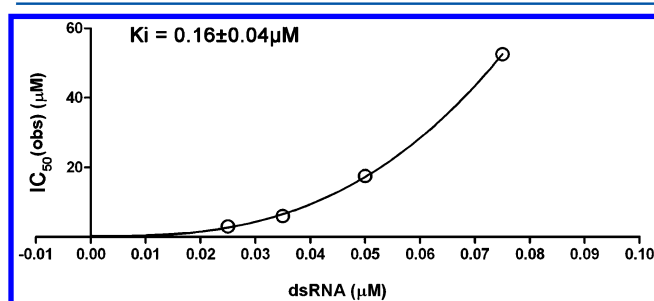

Figure 8. Variation of the inhibitory potency values IC_{50} (obs) for compound **14** against the helicase activity of hDDX3, as a function of the RNA substrate concentration.

(as shown by the increase in $IC_{50(obs)}$ values), according to a competitive mode of action. These results validate the proposed mechanism of inhibition of compound **14** as predicted by the docking studies.

CONCLUSIONS

Owing to the importance of DDX3 as potential new therapeutic target, information regarding its RNA binding site is of prime relevance. Structural studies have been hampered due to the lack of the X-ray crystal structure of hDDX3 in its RNA-bound closed conformation. In this study, based on a closer homologue with good resolution (Drosophila Vasa, PDB code: 2DB3, 2.20 Å), we constructed a three-dimensional model of hDDX3 in complex with RNA. The main aim of this study was to provide relevant information on the RNA binding pocket of this receptor, which can be used for the discovery of novel helicase DDX3 inhibitors. The structural model was subsequently used to screen in silico for new hDDX3 helicase inhibitors. As a result, several of the selected molecules showed substantial potency, confirming the validity of the proposed model. Furthermore, the detailed interactions between hDDX3 and its inhibitors were characterized by molecular docking analysis, which helped us to identify the most

important residues at the basis of the anti-DDX3 activities. Elucidation of these molecular characteristics will help in understanding the structural basis of ligand binding to hDDX3 protein and pave new ways toward broad spectrum antiviral agents.

ASSOCIATED CONTENT

⑤ Supporting Information

The Supporting Information is available free of charge on the ACS Publications website at DOI: 10.1021/acs.jcim.5b00419.

Figures S1−S7, Table S1, molecular dynamics methods, and results (PDF)

AUTHOR INFORMATION

Corresponding Author

*E-mail: botta.maurizio@gmail.com. Phone: +39 0577 234306. Fax: +39 0577 234306.

Notes

The authors declare no competing financial interest.

Present addresses

‖L. B.: Dipartimento di Farmacia, Università di Napoli "Federico II", via D. Montesano 49, 80131, Napoli, Italia.

⊥M. S.: Integrative Pharmacogenomics Institute Level 7, FF3 Building UiTM Puncak Alam Campus 42300 Bandar Puncak Alam Selangor Darul Ehsan. Malaysia, respectively.

ACKNOWLEDGMENTS

REFERENCES

(1) Arhel, N.; Kirchhoff, F. Host Proteins Involved in HIV Infection: New Therapeutic Targets. *Biochim. Biophys. Acta, Mol. Basis Dis.* **2010**, *1802*, 313−321.

(2) Dürr, R.; Keppler, O.; Christ, F.; Crespan, E.; Garbelli, A.; Maga, G.; Dietrich, U. Targeting Cellular Cofactors in HIV therapy. *Top. Med. Chem.* **2014**, *15*, 183−222.

(3) Tintori, C.; Brai, A.; Fallacara, A. L.; Fazi, R.; Schenone, S.; Botta, M. Protein-protein Interactions and Human Cellular Cofactors as New Targets for HIV Therapy. *Curr. Opin. Pharmacol.* **2014**, *18*, 1−8.

(4) Park, S. H.; Lee, S. G.; Kim, Y.; Song, K. Assignment of a Human Putative RNA Helicase Gene, DDX3, to Human X Chromosome Bands p11.3−> p11.23. *Cytogenet. Genome Res.* **1998**, *81*, 178−179.

(5) Yedavalli, V. S.; Neuveut, C.; Chi, Y. H.; Kleiman, L.; Jeang, K. T. Requirement of DDX3 DEAD Box RNA Helicase for HIV-1 Rev-RRE Export Function. *Cell* **2004**, *119*, 381−392.

(6) Ishaq, M.; Hu, J.; Wu, X.; Fu, Q.; Yang, Y.; Liu, Q.; Guo, D. Knockdown of Cellular RNA Helicase DDX3 by Short Hairpin RNAs Suppresses HIV-1 Viral Replication Without Inducing Apoptosis. *Mol. Biotechnol.* **2008**, *39*, 231−238.

(7) Soto-Rifo, R.; Rubilar, P. S.; Ohlmann, T. The DEAD-box Helicase DDX3 Substitutes for the Cap-Binding Protein eIF4E to Promote Compartmentalized Translation Initiation of the HIV-1 Genomic RNA. *Nucleic Acids Res.* **2013**, *41*, 6286−6299.

(8) Soto-Rifo, R.; Rubilar, P. S.; Limousin, T.; de Breyne, S.; Décimo, D.; Ohlmann, T. DEAD-box Protein DDX3 Associates with eIF4F to Promote Translation of Selected mRNAs. *EMBO J.* **2012**, *31*, 3745−3756.

(9) Ariumi, Y. Multiple Functions of DDX3 RNA Helicase in Gene Regulation, Tumorigenesis, and Viral Infection. *Front. Genet.* **2014**, *5*, 423.

(10) Li, C.; Ge, L. L.; Li, P. P.; Wang, Y.; Dai, J. J.; Sun, M. X.; Huang, L.; Shen, Z. Q.; Hu, X. C.; Ishag, H.; Mao, X. Cellular DDX3 Regulates Japanese Encephalitis Virus Replication by Interacting with Viral Untranslated Regions. *Virology* **2014**, *449*, 70−81.

(11) Khadka, S.; Vangeloff, A. D.; Zhang, C.; Siddavatam, P.; Heaton, N. S.; Wang, L.; Sengupta, R.; Sahasrabudhe, S.; Randall, G.; Gribskov, M.; Kuhn, R. J.; Perera, R.; LaCount, D. J. A Physical Interaction Network of Dengue Virus and Human Proteins. *Mol. Cell. Proteomics* **2011**, *12*, M111.012187.

(12) Högbom, M.; Collins, R.; van den Berg, S.; Jenvert, R. M.; Karlberg, T.; Kotenyova, T.; Flores, A.; Karlsson Hedestam, G. B.; Schiavone, L. H. Crystal Structure of Conserved Domains 1 and 2 of the Human DEAD-box Helicase DDX3X in Complex with the Mononucleotide AMP. *J. Mol. Biol.* **2007**, *372*, 150−159.

(13) Schütz, P.; Karlberg, T.; van den Berg, S.; Collins, R.; Lehtiö, L.; Högbom, M.; Holmberg-Schiavone, L.; Tempel, W.; Park, H. W.; Hammarström, M.; Moche, M.; Thorsell, A. G.; Schüler, H. Comparative Structural Analysis of Human DEAD-box RNA helicases. *PLoS One* **2010**, *5*, e12791.

(14) Maga, G.; Falchi, F.; Garbelli, A.; Belfiore, A.; Witvrouw, M.; Manetti, F.; Botta, M. Pharmacophore Modeling and Molecular Docking Led to the Discovery of Inhibitors of Human Immunodeficiency Virus-1 Replication Targeting the Human Cellular Aspartic Acid-Glutamic Acid-Alanine-Aspartic Acid Box Polypeptide 3. *J. Med. Chem.* **2008**, *51*, 6635−6638.

(15) Garbelli, A.; Radi, M.; Falchi, F.; Beermann, S.; Zanoli, S.; Manetti, F.; Dietrich, U.; Botta, M.; Maga, G. Targeting the Human DEAD-box Polypeptide 3 (DDX3) RNA Helicase as a Novel Strategy to Inhibit Viral Replication. *Curr. Med. Chem.* **2011**, *18*, 3015−3027.

(16) Maga, G.; Falchi, F.; Radi, M.; Botta, L.; Casaluce, G.; Bernardini, M.; Irannejad, H.; Manetti, F.; Garbelli, A.; Samuele, A.; Zanoli, S.; Esté, J. A.; Gonzalez, E.; Zucca, E.; Paolucci, S.; Baldanti, F.; De Rijck, J.; Debyser, Z.; Botta, M. Toward the Discovery of Novel Anti-HIV Drugs. Second-Generation Inhibitors of the Cellular ATPase DDX3 with Improved Anti-HIV Activity: Synthesis, Structure-Activity Relationship Analysis, Cytotoxicity Studies, and Target Validation. *ChemMedChem* **2011**, *6*, 1371−1389.

(17) Yedavalli, V. S.; Zhang, N.; Cai, H.; Zhang, P.; Starost, M. F.; Hosmane, R. S.; Jeang, K. T. Ring Expanded Nucleoside Analogues Inhibit RNA Helicase and Intracellular Human Immunodeficiency Virus Type 1 Replication. *J. Med. Chem.* **2008**, *51*, 5043−51.

(18) Università degli studi di Siena; Consiglio Nazionale delle Ricerche, Roma. Radi, M.; Botta, M.; Falchi, F.; Maga, G.; Baldanti, F.; Paolucci, S. Compounds with DDX3 Inhibitory Activity and Uses Thereof. US2012202814, 2012.

(19) Radi, M.; Falchi, F.; Garbelli, A.; Samuele, A.; Bernardo, V.; Paolucci, S.; Baldanti, F.; Schenone, S.; Manetti, F.; Maga, G.; Botta, M. Discovery of the First Small Molecule Inhibitor of Human DDX3 Specifically Designed to Target the RNA Binding Site: Towards the Next Generation HIV-1 Inhibitors. *Bioorg. Med. Chem. Lett.* **2012**, *22*, 2094−2098.

(20) Sengoku, T.; Nureki, O.; Nakamura, A.; Kobayashi, S.; Yokoyama, S. Structural Basis for RNA Unwinding by the DEAD-box protein Drosophila Vasa. *Cell* **2006**, *125*, 287−300.

(21) *Schrödinger Release 2014-3: Maestro*;, version 9.9 Schrödinger, LLC: New York, NY, 2014.

(22) Jorgensen, W. L.; Maxwell, D. S.; Tirado-Rives, J. Development and Testing of the OPLS All-Atom Force Field on Conformational Energetics and Properties of Organic Liquids. *J. Am. Chem. Soc.* **1996**, *118*, 11225−11236.

(23) Wolber, G.; Langer, T. LigandScout: 3-D Pharmacophores Derived from Protein-Bound Ligands and Their Use as Virtual Screening Filters. *J. Chem. Inf. Model.* **2005**, *45*, 160−169.

(24) Verdonk, M. L.; Cole, J. C.; Hartshorn, M. J.; Murray, C. W.; Taylor, R. D. Improved Protein-Ligand Docking Using GOLD. *Proteins: Struct., Funct., Genet.* **2003**, *52*, 609−623.

(25) Cole, J. C.; Nissink, J. W. M.; Taylor, R. Protein-Ligand Docking and Virtual Screening with GOLD. In *Virtual Screening in Drug Discovery*; Shoichet, B., Alvarez, J., Eds.; Taylor & Francis CRC Press: Boca Raton, Florida, USA, 2005.

(26) *PyMOL Molecular Graphics System*, Version 0.99; Schrödinger, LLC: New York, NY, USA, 2011.

(27) Bono, F.; Ebert, J.; Lorentzen, E.; Conti, E. The Crystal Structure of the Exon Junction Complex Reveals how it Maintains a Stable Grip on mRNA. *Cell* **2006**, *126*, 713−725.

(28) Goodford, P. J. A Computational Procedure for Determining Energetically Favorable Binding Sites on Biologically Important Macromolecules. *J. Med. Chem.* **1985**, *28*, 849−857.

(29) Bleicher, K. H.; Böhm, H. J.; Müller, K.; Alanine, A. I. Hit and Lead Generation: Beyond High-Throughput Screening. *Nat. Rev. Drug Discovery* **2003**, *2*, 369−378.